Dynamically updated digital twin for prognostics and health management: Application in permanent magnet synchronous motor

Chinese Journal of Aeronautics, (2024), xxx(xx): xxx–xxx

Chinese Society of Aeronautics and Astronautics
& Beihang University

Chinese Journal of Aeronautics

cja@buaa.edu.cn
www.sciencedirect.com

FULL LENGTH ARTICLE

Dynamically updated digital twin for prognostics and health management: Application in permanent magnet synchronous motor

Haoyu GUO [a,b,c,d], Shaoping WANG [a,b,d,*], Jian SHI [a,b,d], Tengfei MA [a], Giorgio GUGLIERI [c], Rujun JIA [a], Fausto LIZZIO [c]

[a] *School of Automation Science and Electrical Engineering, Beihang University, Beijing 100191, China*
[b] *Tianmushan Laboratory, Hangzhou 310023, China*
[c] *Department of Mechanical and Aerospace Engineering, Polytechnic University of Turin, Turin 10129, Italy*
[d] *Beihang Ningbo Research Institute, Ningbo 315800, China*

Received 1 June 2023; revised 16 July 2023; accepted 18 October 2023

KEYWORDS

Digital Twin (DT);
Dynamic Update;
Independence Principle;
Multi-field Coupling;
Permanent Magnet Synchronous Motor (PMSM);
Prognostics and Health Management (PHM)

Abstract Current research on Digital Twin (DT) based Prognostics and Health Management (PHM) focuses on establishment of DT through integration of real-time data from various sources to facilitate comprehensive product monitoring and health management. However, there still exist gaps in the seamless integration of DT and PHM, as well as in the development of DT multi-field coupling modeling and its dynamic update mechanism. When the product experiences long-period degradation under load spectrum, it is challenging to describe the dynamic evolution of the health status and degradation progression accurately. In addition, DT update algorithms are difficult to be integrated simultaneously by current methods. This paper proposes an innovative dual loop DT based PHM framework, in which the first loop establishes the basic dynamic DT with multi-filed coupling, and the second loop implements the PHM and the abnormal detection to provide the interaction between the dual loops through updating mechanism. The proposed method pays attention to the internal state changes with degradation and interactive mapping with dynamic parameter updating. Furthermore, the Independence Principle for the abnormal detection is proposed to refine the theory of DT. Events at the first loop focus on accurate modeling of multi-field coupling, while the events at the second loop focus on real-time occurrence of anomalies and the product degradation trend. The interaction and collaboration between different loop models are also discussed. Finally, the Permanent Magnet Synchronous Motor (PMSM) is used to verify the proposed method. The results show that the modeling method proposed can accurately track the lifecycle per-

* Corresponding author.
E-mail address: shaopingwang@buaa.edu.cn (S. WANG).

Peer review under responsibility of Editorial Committee of CJA.

Production and hosting by Elsevier

https://doi.org/10.1016/j.cja.2023.12.031

Please cite this article in press as: GUO H et al. Dynamically updated digital twin for prognostics and health management: Application in permanent magnet synchronous motor, *Chin J Aeronaut* (2024), https://doi.org/10.1016/j.cja.2023.12.031

formance changes of the entity and carry out remaining life prediction and health management effectively.

1. Introduction

Due to the significant impacts of product degradation and failure, such as production disruptions, safety hazards, and higher maintenance costs, the Prognostics and Health Management (PHM) technology is widely used in aerospace system. Through real time monitoring the product states, PHM can detect product performance degradation, predict remaining life and diagnose the fault. However, the progress and development of product degradation are difficult to reflect from externally detectable sensors, which are the result of internal states changes with the coupling effect of multiple fields. Therefore, it is vital to develop effective health monitoring techniques that can characterize the internal changes under load action. Coincidentally, the Digital Twin (DT) method has emerged, and has received increasing attention through creating a high-fidelity digital mirror of physical entity.[1] Michael[2] is credited with proposing DT as a solution for complex product operations. The aim of DT is to establish a virtual representation that mirrors the physical entity,[3] enabling the tracking of state variables and parameter changes. On the other aspect, the development of multi-filed coupling modeling provides more detailed possibilities for digital representation of the product internal state. DT have the potential to monitor the state, manage the lifecycle, and optimize decision-making for the physical entity. The integration of the Internet of Things (IoT) and information systems also brings new energy to the parallel interaction between the physical and cyber domains. Consequently, DT can be seen as highly precise integrated sensors, capturing and representing a wealth of data from physical entities in a virtual environment. Hence, DT-based PHM was first adopted in the aerospace industry,[4] which not only changes with changes in physical entity through real time updating DT parameters, but also reflects the changes in the internal state of the product under working conditions.

Although DT can synchronously change with changes of physical entity in an ideal state, product degradation is related to multiple factors, and the variation law is very complex in real practice. The synchronous evolution DT is difficult to accurately describe the product lifecycle changes through the entire service life. This paper presents a dual loop DT-PHM framework to perform accurate internal state monitoring and product degradation characterization through real time data updating from physical entities to their virtual counterparts. In the first loop, the virtual replica system of physical product is established through gathering the data by sensors, updating the DT and mapping the virtual model. When the process of product starts degradation, the DT-based PHM model is switched to the second loop through abnormal detection. The real time data is fed into the DT-based PHM according to the degradation state from time to time, and the entire process DT-based PHM model enables a nearly accurate representation during the lifecycle operation through dynamical updating of parameters. The DT-based PHM can foresee probable future issues, and decrease product faults and unnecessary maintenance. In the process of abnormal detection, a theory of Independent Principle is proposed, which supplements the theoretical system of DT. In this way, DT-based PHM evolves from multi-filed coupling, thus optimizing the updating parameters, increasing the precision of health state recognition and remaining useful life estimation. The Permanent Magnet Synchronous Motor (PMSM) is used to validate the framework and simulate the wide range of scenarios during the entire operation process. The results show that the PHM DT helps to improve the reliability and maintenance efficiency of complex product. Compared with previous research, the proposed DT-based PHM can accurately describe the working behaviors of the physical entity and the accuracy is improved compared with that of the previous methods.

The contributions of this study are highlighted as follows:

(1) Considering the difference between normal state DT and degradation DT of product, a dual loop DT based PHM framework is provided, in which the first loop provides the Basic DT (BDT) based on the dynamic updating, and the second loop focuses on the DT-based PHM (PHM-DT) for characterizing the degradation process of product through monitoring the changes in health status.
(2) The BDT and PHM-DT interaction updates through abnormal detection based on the "Independent Principle", which is a significant contribution to the theory of DT. With regular real-time updates, the comprehensiveness and accuracy of the interaction will steadily increase over time.

At the end of this paper, we validate our approach based on a case study of PMSM. Compared with traditional prediction methods, the method proposed in this paper can better accompany the characteristic change of the entity and the accuracy is improved by about 37%. The rest of the paper is organized as follows: Section 2 introduces the research related to DT and PHM; Section 3 describes the dual closed-loop DT-based PHM framework; Section 4 introduces the DT updates mechanism; Section 5 carries out the case study on PMSM; Section 6 gives conclusions.

2. Related work

2.1. Modeling of DT

Back in 2011, NASA experts presented the three-dimensional DT that included the physical entity, DT and their bridge, in which the information generated in the physical world was gathered to create and implant DT. This approach emphasizes seamless integration of the IoT and information systems. By harnessing advanced information interaction technologies,

Please cite this article in press as: GUO H et al. Dynamically updated digital twin for prognostics and health management: Application in permanent magnet synchronous motor, *Chin J Aeronaut* (2024), https://doi.org/10.1016/j.cja.2023.12.031

industrial sectors have been pushed towards greater levels of informatization, digitization, and intelligence. This convergence holds immense potential for driving efficiency, innovation, and optimization across various industries.[5] Sensors and other devices that collect accurate data on the state of process provide the real time updating strategy to replicate what actually occurs. Building mathematical DT with a sufficient level of complexity are important to forecast real-life behaviors in various contexts.

Many manufacturers have already applied the DT concept to actual production. In order to improve the design performance of the product, Marr developed DT for vehicles, which helps to realize the optimal design through information interaction between the vehicle and the factory.[6] Boeing CEO said that as we enter the next decade, DT, due to its potential for increased efficiency and improved performance, holds promise for revolutionizing global aircraft manufacturing. In the realm of manufacturing, companies, such as Siemens[7] and the F-35 manufacturer Lockheed Martin,[8] are increasingly building virtual workshops and digital factories to map physical spaces into cyberspace. This innovation holds potential for streamlining operations, optimizing resource allocation, and enhancing collaboration.

By now, the industrial application of DT technology is mainly concentrated in the fields of production, design, and prediction.[9] DT modeling methods are mainly divided into four types: Finite Element Modeling (FEM), multidisciplinary modeling language, neural network, and mathematical model. Tao et al. [10] defined DT as the all-factor reconstruction and digital mapping of the operational state and operational progress of the physical entity and also information space of the product. Fan et al. [11] proposed a DT visualization architecture for Flexible Manufacturing Systems (FMS), and explored modeling multi-source heterogeneous information. Dang et al. [12] proposed a DT framework based on cloud computing and deep learning, taking bridge as objects to establish DT. Castellani et al. [13] used the Modelica language to build a DT of a company's power, heating, ventilation and air conditioning systems, and obtained the normal working data of the actual system through the operation of the established DT. Wang et al.[14] established a DT of the image convolutional neural network of the welding process, and obtained the current penetration information by acquiring the weld pool image and current data. Venkatesan et al. [15] developed a neural network DT that conforms to the running state of the motor according to the running time, distance of the vehicle and the health state of the onboard motor. Moghadam et al. [16] established a torsional dynamic DT for offshore wind turbines, and gave a related parameter estimation algorithm. Li et al. [17] proposed an adaptive extension-based filter that is robust and accurate in estimating DT parameters for both Li-ion and Lead-acid batteries in the state of charge. Lei et al. [18] took the entire thermal power plant as the object, and studied the four-layer architecture about 3D modeling, mathematical modeling, rendering and real time monitoring. Hu et al. [19] constructed a high-precision gas turbine DT, introduced an error module and kernel density estimation self-learning to optimize the update of DT, and carried out fault status diagnosis of the gas turbine based on this method.

2.2. PHM based on DT

PHM takes center stage in the Industry 4.0 revolution, where the key challenges involve accurately detecting whether equipment is operating normally and predicting when faults may occur. Effective implementation of PHM holds the potential to minimize the occurrence of catastrophic failures and reduce costs associated with scheduled maintenance. Given the complexity of understanding internal state changes during degradation, DT emerges as a promising method to characterize the internal health state across different fields and objects. Leveraging its technical advantages, DTs enable better monitoring and analysis of the health conditions of products, leading to improved prognostics and decision-making processes. Bai et al. [20] proposed a novel 3D multi-physics DT for proton exchange membrane fuel cell based on the Proper Orthogonal Decomposition (POD) method, and exhibited and analyzed the DT results of voltage, temperature, membrane water content and liquid water saturation fields. Ye et al. [21] proposed a reconfigurable Dynamic Bayesian Networks (DBN) method that can capture interactions between damages. Their study shows via a numerical example that the reconfigurable DBN can accurately predict the crack growth acceleration caused by bolt loosening. The method tracks multiple damages and has good physical interpretability. Li et al. [22] proposed a PHM system based on advanced DT technology for the Five-hundred-meter Aperture Spherical radio Telescope (FAST). The PHM system utilizes finite element analysis of the DT to evaluate the safety status and predict the fatigue life of FAST's cable-net structure, enabling effective Condition-Based Maintenance (CBM) and ensuring the healthy and safe operation of the structure while improving maintenance efficiency and reducing costs. Angjeliu et al. [23] established a FEM DT for the Milan Cathedral, which can predict the future damage trend of the building structure through the analysis of the FEM. Liu et al. [24] took High-Speed Permanent Magnet Motor (HSPMM) as an example, and comprehensively discussed the issues that need to be considered in the construction of a multidisciplinary DT of HSPMM and the fault diagnosis of its electrical drive system. Aivaliotis et al. [25] presented a methodology for calculating machinery equipment's Remaining Useful Life (RUL) using physics-based simulation models and the DT concept, enabling predictive maintenance for manufacturing resources. This method involves modeling resources, gathering data from machine controllers and sensors for tuning digital models, and using simulation results to assess the condition and calculate RUL, and allows for non-invasive monitoring and prediction of machine status. Their methodology is validated through a case study on predicting the RUL of an industrial robot. Oluwasegun et al. [26] proposed a conceptual framework for applying the DT technology to predict the control element drive mechanism and a data-driven method for abnormal detection by using coil current curves to optimize the operation and maintenance process of nuclear power plants. Peng et al. [27] conducted research on the core technology of DT structural rolling bearings, including detection, modeling and PHM technology, and analyzed the challenges and future research directions in the development of rolling bearing DT technology. Booyse et al. [28] proposed to use the form of deep DT, which learns from the

distribution of health data, and uses its advantage of independence from historical failure data to estimate asset health. Correa-Jullian et al. [29] discussed the core aspects of the design, development, and implementation of data-driven PHM applications, and demonstrated that they can improve reliability evaluation in liquid hydrogen storage systems. Based on DT's PHM idea, Candon et al. [30] gave a comprehensive study on DT in the form of machine learning models for aircraft load monitoring, including linear regression models, traditional artificial neural networks, and deep learning strategies. They also discussed the need for time-series modeling and explored potential solutions to the issues encountered in traditional or modern aircraft data acquisition systems. Their findings hold significant value for researching fatigue problems in mechanical systems.

Of all the existing works mentioned above, the DT-PHM methods have the following core limitations: firstly, the established DTs are discipline-specific, limiting their ability to comprehensively describe the equipment's state; secondly, the physical interpretation of parameters in DT, built using multidisciplinary language, neural network models, or finite element methods, is unclear; thirdly, the established DTs are open-loop models, lacking a corrective feedback loop for comparison; lastly, most of the DTs are based on fixed-parameter models, unable to adapt to changes in actual equipment states. Therefore, the focus of this paper is to establish a multidisciplinary coupling DT and its dynamic update mechanism. Moreover, DT is combined with PHM to build a general DT operation and maintenance framework.

3. Dual loop DT based PHM framework

With the long-term operation of actual equipment, the digital model established according to traditional simulation has a certain risk of errors. Due to the factors such as degradation or failure, the parameters or the model will change accordingly, resulting in deviation of DT performance from the entity. Therefore, a closed-loop comparison link is needed to ensure the consistency of the DT with the actual equipment. The two main aspects of DT research are "establishment" and its "application". Based on this point, this paper presents a dual closed-loop DT-based PHM framework, as shown in Fig. 1.

(1) First Loop: Basic DT

The first loop is used to establish the virtual model of the physical product under the normal condition that consists of four parts: physical entity, IoT, DT, and DT correction. The physical entity serves as the foundation for DT modeling, and acts as the starting point for the DT system. IoT establishes a data interconnection between the physical space and virtual space. This information connection provides the necessary "data nutrients" required for the dynamic updating of the DT system. DT modeling serves as the essence of DT, encapsulating its very soul. Dynamicity and high accuracy form the core essence of DT. We define DT as a dynamic model, wherein the internal parameters are influenced by its self-state and operating conditions, ensuring a continuous adaptation to changing circumstances.

(2) Second Loop: PHM-DT

The second loop is used to establish the virtual model of product during lifecycle degradation. Here, the PHM is the core of DT. In the second loop, the health status can be detected, faults can be diagnosed, and the remaining useful life can be predicted with PHM-DT. In order to describe the PHM scenarios at different levels, PHM-DT collects the observed information on the physical product, iteratively updates the parameters to the corresponding DT, and integrates comprehensive lifecycle DT. Since the degradation trend of physical entity is closely related to the operational condition and uncertainty factors, the evolution of product status is different under the degradation scenario. In order to capture the degradation state accurately, processing of the integrated data obtained from the physical entity sensors is carried out, and updating of the dynamic parameters is implemented from time to time.

(3) Interaction: Abnormal detection

As the physical entity operates, the DT remains in a dynamic process of adaptation, and needs the model evolution technology to drive self-updating of the virtual model. Abnormal detection is the important interaction between the dual loop DT. In this paper, we put forward a novel concept of "Independence Principle" in the abnormal detection process to ensure the significance of the established DT. The specific principle will be discussed in detail in the next section. This paper transforms from basic DT to PHM-DT with abnormal detection. Abnormal detection can establish the seamless con-

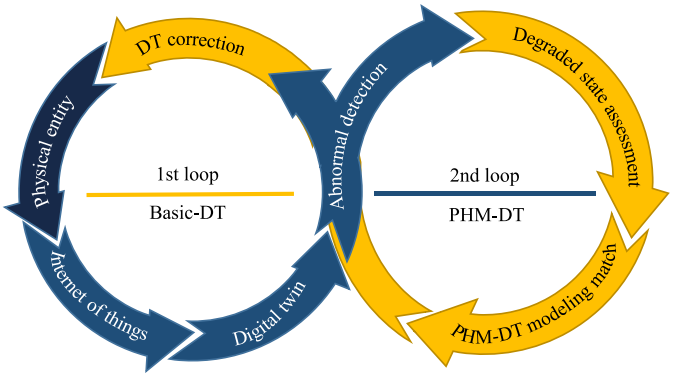

Fig. 1 Dual loop DT based PHM framework.

nection between basic DT and PHM-DT and automatically respond to the changes in product status of entire lifecycle.

3.1. Basic DT modeling (1st loop DT)

In general, a DT is an integrated simulation of a physical entity that encompasses multiple disciplines, such as mechanical and electrical disciplines, across its operation (see Fig. 2). If the operational physical mechanism is known, we should establish the real-time dynamic operation process model of physical entities with multi-field coupling. The basic DT, as the mirror image of physical product, can be established by multi-field coupling modeling.

As shown in Fig. 2, the physical entity and DT share the same input $\boldsymbol{U}$. The actual output from the physical product is represented as $\boldsymbol{O}$. Based on the first-principle structure, the output of basic DT can be shown as

$$\hat{\boldsymbol{O}} = f(x_1, x_2, \cdots, x_m, x_{m+1}, \cdots, x_n, \boldsymbol{U}) + \boldsymbol{D} \tag{1}$$

where $\hat{\boldsymbol{O}}$ is the performance output of DT, $\boldsymbol{U}$ is the input of DT, and $\boldsymbol{D} = [d_1, d_2, \cdots, d_r]$ is the disturbance and uncertainty. The parameters of DT is expressed as $\boldsymbol{X} = [x_1(t), x_2(t), \cdots, x_m(t), x_{m+1}, x_{m+2}, \cdots, x_n]$, in which $[x_1(t), x_2(t), \cdots, x_m(t)]$ varies with the operational condition, and $[x_{m+1}(t), x_{m+2}(t), \cdots, x_n(t)]$ keeps constant like the geometric size. The impact on DT parameters of operational condition can be expressed as

$$x_i(t) = x_0 + q(c_1, c_2, \cdots, c_l) \tag{2}$$

where x_0 is the initial value of the parameter, q represents the operating conditions on the parameters, and $\boldsymbol{C} = [c_1, c_2, \cdots, c_l]$ is the set of condition parameters.

In certain scenarios, model-based approaches may not effectively capture the complexities or uncertainties present in real systems. In such cases, data-driven approaches can be employed to complement the model and enhance its performance. Data-driven methods leverage the analysis and mining of extensive system data to extract valuable patterns, relationships, and laws. By incorporating actual data, these approaches can provide additional insights to improve the accuracy and effectiveness of the model.

By leveraging their respective advantages, they complement one another and aid in joint characterization of the target object. This integration can be mathematically expressed as Eq. (3)

$$\hat{\boldsymbol{O}} = f(\vartheta(\cdot), \eta(\cdot), \boldsymbol{U}) + \boldsymbol{D} \tag{3}$$

where $\vartheta(\cdot)$ represents the model-driven model, $\eta(\cdot)$ represents the data-driven model and the parameters $\boldsymbol{X}$ included in the overall model.

Since the physical mechatronic product operates in multiple disciplines such as mechanical, electrical, control et al., its dynamics, electricity and another part directly affect product performance. When the basic DT is applied to the physical product, multi-field coupling DT is established based on the dynamics equation and Newton's law. In order to promote the application of virtual spaces in the DT establishment, information interaction is responsible for updating the DT parameters collected from entity sensors. It is important to note that when creating a DT for different objects, it is essential to incorporate the relevant disciplines specific to the entities. After establishing the basic DT based on multi-field coupling, its parameter updating mechanism can be shown in Fig. 3.

3.2. PHM based on DT (2nd loop DT)

Although basic DT can accurately map the physical product with the changes under the operating condition, it is difficult to express the physical product corresponding to the full life cycle process. PHM DTs are different in differed health states in 2nd loop DT.

This paper defines the health state index of product as

$$H = 1 - \frac{\sigma_0 - \sigma_t}{\sigma^\tau} \tag{4}$$

where σ_0 represents the initial value of the key parameter, σ_t represents the value of the key parameter at time t, and σ^τ represents the degradation threshold value of the key parameter. The health state index can reflect the degradation degree of product within the range of 0 to 1. Let $H = \{H_1, H_2, \cdots, H_b\}$ represents the product state from complete wellness, minor fault, moderate fault to total failure. By assigning appropriate degradation level to the actual situation, we can effectively determine the operational status of an entity and build the appropriate DT. Fig. 4 shows the PHM based on DT in the 2nd loop DT.

In Fig. 4, PHM-DT modeling results not only form the final insights through model matching, but also realize the co-evolution through model switching updating. For example, if

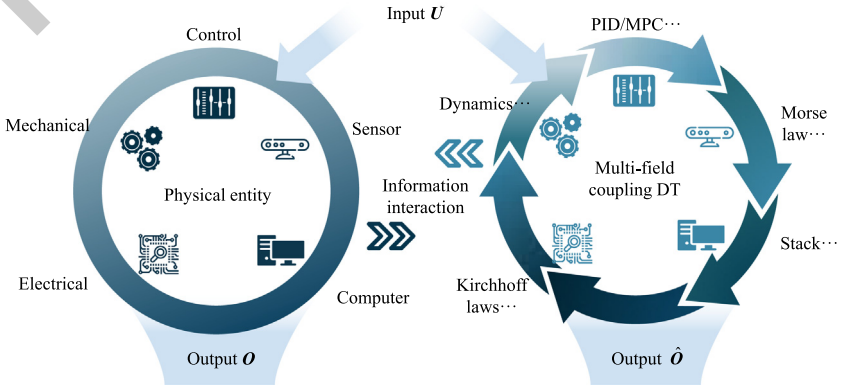

Fig. 2 Basic DT modeling with multiple-field coupling.

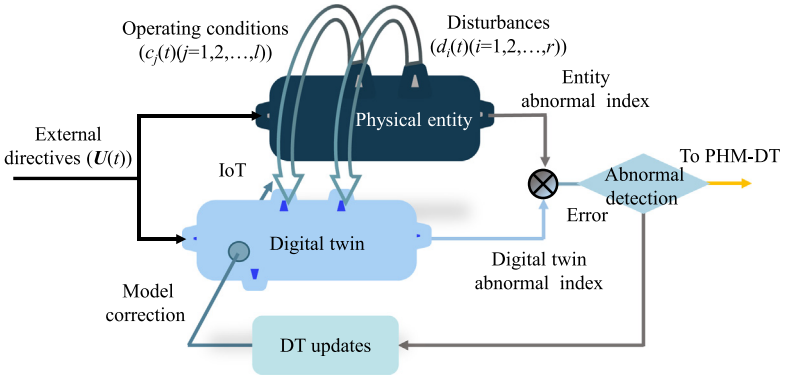

Fig. 3 Basic DT modeling mechanism.

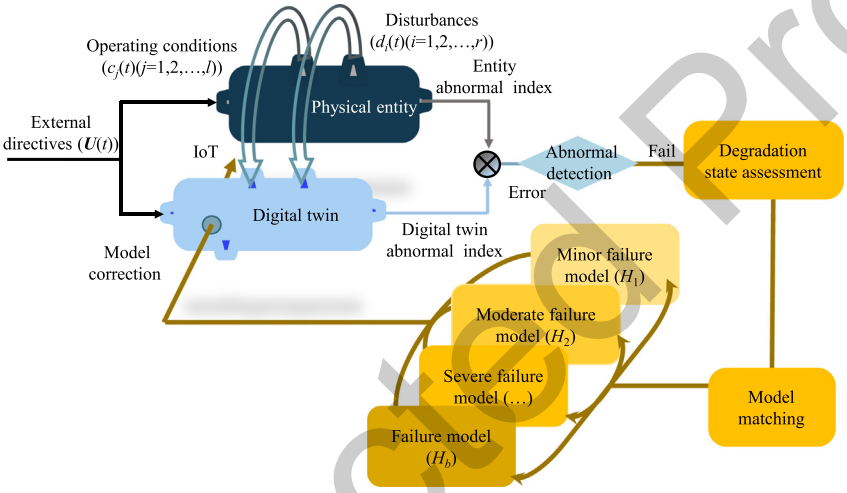

Fig. 4 PHM-DT modeling mechanism.

we divide the health state into five parts, the product health state index can be written as

$$H=\begin{cases}1, \text{Normal}\\ H_1, \text{Minor fault}\\ H_2, \text{Moderate fault}\\ H_3, \text{Severe fault}\\ 0, \text{Failure}\end{cases} \tag{5}$$

The meaning of the health state of product is as follows:

(1) $H=1$ represents the normal state, in which the product has no or a little change without affecting product performance.
(2) $H=H_1$ indicates the minor fault state, in which minor degradation of the product occurs during the operation.
(3) $H=H_2$ expresses the moderate fault state, in which moderate degradation of the product arises after running a considerable period of time.
(4) $H=H_3$ is the severe fault state, in which serious degradation of the product occurs in the late stages of product life.
(5) $H=0$ represents the failure state, which means the product reached its lifespan.

Different health state corresponds to different parameters or models within the DT. Therefore, it is necessary to update the DT based on the current health state of equipment by detecting its status changes. For example, the values of key parameters within the DT may vary through updating the algorithm when the equipment deteriorates from minor fault to moderate fault state. Hence, by employing appropriate algorithms, the DT is updated by considering the current health state of the equipment to ensure its alignment with the physical entity. In the case study of this paper, we utilize the recursive least squares method to update the flux ψ_f, resistances R, and inductance L in the PMSM DT based on the current state of health, which ensures that the DT remains consistent with the entity across different health stages.

In summary, adjusting the parameters or structure of the DT based on the equipment's health state is a crucial step in ensuring its consistency with the actual equipment. By updating the DT using suitable algorithms when the equipment's state changes, the reliability and adaptability of the DT can be enhanced. Such update strategies help monitor and maintain the entity more effectively and provide accurate predictions and decision support.

Please cite this article in press as: GUO H et al. Dynamically updated digital twin for prognostics and health management: Application in permanent magnet synchronous motor, *Chin J Aeronaut* (2024), https://doi.org/10.1016/j.cja.2023.12.031

4. Dynamic update mechanism of dual loop DT based PHM framework

It is obvious that abnormal detection is the most important interaction of dual loop DT based PHM framework. According to the health state of physical entity, abnormal detection can be triggered between BDT and PHM-DT. This paper presents "indices" of abnormal detection as a trigger to update the DT appropriately. Because the indices are independent of product output and internal parameters, we define the idea as "Independence Principle". According to this principle, anomalies in DT should be identified based on "indices", and the DT is subsequently updated based on the characteristic information of the real equipment. In other words, it is not meaningful to directly compare the output or the main parameters between DT and the physical entity, because we can already obtain information about the target by detecting the signals from the entity. The purpose of building DT is not simply to create it, but rather to improve its accuracy by incorporating relevant and independent indices.

As shown in Fig. 3, the differences between DT and entity are initially identified through abnormal indices. If the difference detection is passed, the DT is considered reliable and doesn't require updates, and the output result $\hat{\boldsymbol{O}}$ of the DT can be directly utilized. Once the DT's consistency is confirmed, the corresponding output result can be provided to external sources. If the performance of a physical entity degrades and abnormal detection is triggered, the parameters of the DT are needed to be updated using parameter estimation techniques. Furthermore, if the DT still fails to pass abnormal detection after several parameter updates, it suggests the occurrence of a change in the mechanism or structure of the entity.

Consequently, the DT needs to be remodeled through system identification and other appropriate methods. It is essential for all updated DTs to successfully pass the consistency measure before they can be deemed consistent with the technical state of the physical entity.

4.1. Definition of the trigger based on abnormal indices

Components in actual equipment will degrade or fail as the operating time increases, which will cause the entity to deviate from the state of the DT. To ensure consistency between DT and the entity, we utilize the indices as the triggering criteria. The abnormal trigger is defined as

$$\text{trig} = g(G^0_{\text{entity}}, G^t_{\text{entity}}, G_{\text{DT}}) \tag{6}$$

where G^0_{entity} is the abnormal index at the previous moment of physical entity, G^t_{entity} is the abnormal index at time t of entity, and G_{DT} is the abnormal index at the current moment of DT. When the threshold is not satisfied, the abnormal trigger is initiated, which indicates that the DT needs to be updated. The abnormal trigger is a function that depends on three abnormal indices ($G^0_{\text{entity}}, G^t_{\text{entity}}, G_{\text{DT}}$) selected from the DT system. Its functional relationship can be described by the function $g(\cdot)$. The specific form of $g(\cdot)$ is not fixed, and determining the appropriate pattern for obtaining abnormal triggers based on the abnormal indices requires consideration of different objects and actual situations.

In the following are the guidelines of Independent Principle:

(1) The abnormal factor G_* is a parameter that can effectively characterize the abnormal features between DT and physical entity.
(2) Try to avoid selecting output or key internal parameters as abnormal indices. Since the relevant parameters can already be obtained by traditional means, the existence of parameters derived from DT becomes meaningless.

However, the specific process of selecting these factors should be based on the unique characteristics of the actual equipment. It is essential to consider the factors such as design, functionality, and operational environment of the equipment. By thoroughly understanding these characteristics, we can determine the specific abnormal factors that are most relevant and significant for detecting deviations in the equipment's performance.

4.2. DT updates

For different form DT, parameter updates need to be combined in different ways to achieve the best results. According to the description of the model correction link in the previous chapter, the update of DT can be divided into parameter update and model update. For linear models, the Recursive Least Square (RLS), Gradient Descent (GD), and Conjugate Gradient (CG) can be used to update parameters. For nonlinear models, model parameters can be updated using Particle Swarm Optimization (PSO), Maximum Likelihood estimation (ML), Artificial Neural Networks (ANN), and other methods.

Taking the RLS algorithm as an example, consider the linear model. We can assume that there exists a relationship between the variable parameters and their observed values, which can be represented as

$$\boldsymbol{Z}_t = \boldsymbol{Q}_t\boldsymbol{\theta} + \boldsymbol{V}_t \quad t = 1, 2, \cdots, l \tag{7}$$

where $\boldsymbol{Z}_t$ represents an observation output vector consisting of $\boldsymbol{Z}(t)$, t represents the observation at the t^{th} step, $\boldsymbol{Q}_t$ represents an observation vector consisting of t state values, $\boldsymbol{\theta} = [x_1, x_2, \ldots, x_m]^{\text{T}}$ represents the parameter that requires updating, l is the number of observation, and $\boldsymbol{V}_t$ refers to the uncertainty term or perturbation.

The estimation algorithm of RLS parameters is

$$\begin{cases} \boldsymbol{K}_{t+1} = \boldsymbol{P}_{t+1}\boldsymbol{q}^{\text{T}}(t+1) \times [\lambda + \boldsymbol{q}(t+1)\boldsymbol{P}_t\boldsymbol{q}^{\text{T}}(t+1)]^{-1} \\ \boldsymbol{P}_{t+1} = \frac{1}{\lambda}[\boldsymbol{P}_t - \boldsymbol{K}_{t+1}\boldsymbol{q}(t+1)\boldsymbol{P}_t] \\ \hat{\boldsymbol{\theta}}_{t+1} = \hat{\boldsymbol{\theta}}_t + \boldsymbol{K}_{t+1}\left[\boldsymbol{Z}(t+1) - \boldsymbol{q}(t+1)\hat{\boldsymbol{\theta}}_t\right] \end{cases} \tag{8}$$

where $\boldsymbol{K}_{t+1}$ is the correction gain; $\boldsymbol{q}(t)$ is the t^{th} observation, and is an element of $\boldsymbol{Q}_t$; $\hat{\boldsymbol{\theta}}_t$ is the estimated value of the parameter at the t^{th} step of $\boldsymbol{\theta}$; $\boldsymbol{Z}(t)$ is the measured value at the t^{th} step, and is an element of $\boldsymbol{Z}_t$; $\boldsymbol{P}_{t+1}$ is the prediction of the $(t+1)^{\text{th}}$ step based on the measurement at the previous step, and $\boldsymbol{P}_0$ needs to be preset with a suitable initial value; λ is forgetting factor. The parameters can be updated through iterative updates using this method.

In the linear model, parameter $\hat{\boldsymbol{\theta}}_t$ can be updated iteratively using Eq. (8) to gradually approach the true value of the parameter. This iterative updating process allows for refining

the parameter result and reducing the discrepancy between the estimated and actual values.

As non-linear models, taking the PSO algorithm as an example, we define the objective function as

$$\chi(\boldsymbol{\theta}) = \pi(\boldsymbol{\theta}) \cdot \mathrm{sign}(\pi(\boldsymbol{\theta})) \tag{9}$$

where $\pi(\cdot)$ represents the deviation function between the entity observation and the DT result observation, and $\mathrm{sign}(\cdot)$ is a symbolic function. In the context mentioned, the deviation function can be defined as $\pi(\boldsymbol{\theta}) = \boldsymbol{Z} - \hat{\boldsymbol{O}}$. The task of PSO is to find the minimum value $\chi(\boldsymbol{\theta})$, and determine the zero solution for $\boldsymbol{\theta}$. The resulting solution represents the optimal parameter that satisfies the entity observation conditions. Therefore, the objective function is denoted as $\chi(\boldsymbol{\theta}) = (\boldsymbol{Z} - \hat{\boldsymbol{O}}) \cdot \mathrm{sign}(\boldsymbol{Z} - \hat{\boldsymbol{O}})$. The PSO algorithm can be used to obtain the minimum value of $\chi(\boldsymbol{\theta})$ and the resulting solution.

The parameters that need to be updated in the non-linear models are $\boldsymbol{\theta} = [x_1, x_2, \ldots, x_m]^{\mathrm{T}}$. The iterative update of the optimal solution is shown in Eq. (10).

$$\begin{cases} v_i^{k+1} = \omega v_i^k + c_1 r_{i1}^k (\kappa_i^k - x_i^k) + c_2 r_{i2}^k (\kappa_g^k - x_i^k) \\ x_i^{k+1} = x_i^k + v_i^{k+1} \end{cases} \tag{10}$$

where v_i^k represents the speed of the i^{th} particle at the k^{th} iteration, with the initialization speed being 0; ω denotes the inertia weight, which controls the impact of the particle's previous velocity on the current velocity; c_1 represents the individual learning factors, typically assigned a value of 2; and it determines how much a particle relies on its own best solution; c_2 is the social learning factor, also typically set to 2. and it decides how much a particle considers the global best solution found by all particles; r_1 and r_2 are random numbers with the values ranging from 0 to 1; κ_i^k refers to the optimal target solution obtained by the i^{th} particle as of the k^{th} iteration; κ_g^k represents the optimal target solution found by all particles up to the k^{th} iteration; x_i^k denotes the solution corresponding to all particles at the k^{th} iteration.

By assigning appropriate values to these variables and applying them within the PSO algorithm, it becomes possible to optimize the search for the optimal solutions in a multi-dimensional space. It is important to note that PSO may produce multiple sets of solutions that meet the objective function. Therefore, it is necessary to filter the obtained solutions based on the specific situation and select the parameter set that best fits the actual situation as the updated value. Hence, selecting an appropriate updating method for DT requires considering the complexity of the model, the nature of the data, and the desired optimization objectives. By taking these factors into account, we can achieve the best results in updating DT parameters and updating accuracy and performance.

4.3. Consistent measurement

It is crucial to verify and compare the output characteristics of the DT with those of the actual equipment to ensure its effectiveness and accuracy. This validation process is necessary to confirm that the updated DT appropriately reflects the state of the entity. By assessing the similarity between the updated DT and the entity, we can ensure the reliability of the degradation assessment.

The Mahalanobis Distance (MD) is a commonly employed algorithm in machine learning for measuring the dissimilarity between two samples. It calculates the difference by considering the covariance between variables. However, a disadvantage of MD is its tendency to amplify the influence of variables with small changes. This feature can be considered as an advantage in monitoring the disparity between the updated DT and the entity.

We define state vectors and a set of vectors as follows:

$$\begin{cases} \boldsymbol{\theta}_w = [x_{1w}, x_{2w}, \ldots, x_{mw}]^{\mathrm{T}} \\ \boldsymbol{X} = [\boldsymbol{\theta}_1, \boldsymbol{\theta}_2, \ldots, \boldsymbol{\theta}_v, \boldsymbol{\theta}_{\mathrm{DT}}] \end{cases} \tag{11}$$

where $\boldsymbol{\theta}_w$ represents the state matrix composed of ω measurements of the entity; $\boldsymbol{\theta}_{\mathrm{DT}}$ is the running state vector value of DT; $\boldsymbol{X}$ consists of DT and v entity state vectors under the same working condition. In calculating the MD, the number of the sample size is required to be greater than the number of dimensions of the sample, that is $v + 1 > m$. The mean of these v entity state vectors is defined as

$$\boldsymbol{\mu}_\alpha = \frac{1}{v}(\boldsymbol{\theta}_1 + \boldsymbol{\theta}_2 + \ldots + \boldsymbol{\theta}_v) \tag{12}$$

Let matrix $\boldsymbol{D}$ be the inverse of the transposed covariance of $\boldsymbol{X}$, as shown as follows:

$$\boldsymbol{D} = \mathrm{Cov}(\boldsymbol{X}^{\mathrm{T}})^{-1} \tag{13}$$

Therefore, the MD between $\boldsymbol{\mu}_\alpha$ and $\boldsymbol{\theta}_{\mathrm{DT}}$ is

$$\mathrm{MD} = \sqrt{(\boldsymbol{\mu}_\alpha - \boldsymbol{\theta}_{\mathrm{DT}})^{\mathrm{T}} \boldsymbol{D} (\boldsymbol{\mu}_\alpha - \boldsymbol{\theta}_{\mathrm{DT}})} \tag{14}$$

We need to set a threshold ε based on actual experience. When $\mathrm{MD} < \varepsilon$, it is considered that the updated DT has a high state consistency with the entity; if $\mathrm{MD} > \varepsilon$, it is considered that the DT still needs to be updated. It is important to note that validation of the model is required after update of the parameters and structure.

5. Case study: PMSM

The PMSM is a highly integrated and multi-filed electromechanical device that serves a crucial role in energy transformation through electric energy. The accurate modeling and coupling of its multiple disciplines are essential for establishing the DT based model. This paper focuses on developing a comprehensive DT for a surface-mounted PMSM that takes into account various disciplines, including electricity, control, dynamics, power loss, and thermal aspects. The DT is established by combining both model-driven and data-driven fusion techniques.

5.1. Multi-filed modeling of PMSM

5.1.1. Electrical & dynamics models of PMSM

The classical PMSM's d-q voltage mathematical model (model-driven) with uncertainty are

$$\begin{cases} u_d = R i_d + L_d \frac{\mathrm{d}i_d}{\mathrm{d}t} - \omega_e L_q i_q + \delta_d \\ u_q = R i_q + L_q \frac{\mathrm{d}i_q}{\mathrm{d}t} + \omega_e (L_d i_d + \psi_f) + \delta_q \end{cases} \tag{15}$$

where u_d, u_q are the d-q components of the stator voltage; i_d and i_q are the d-q axis components of the stator current; R is the resistance of the stator; L_d and L_q are the d-q components of the inductance components; ω_e is the electrical angular velocity; ψ_f is the permanent magnet flux; δ_d and δ_q are the uncertainty of the voltage equation, which are used to ensure the accuracy of PMSM DT and are the basis for parameter identification.

The equation for the electromagnetic torque is shown as follows:

$$T_e = \frac{3}{2} P_n i_q \psi_f \tag{16}$$

where P_n is the number of pole pairs of the PMSM. The dynamics equation of the PMSM is

$$T_e = T_m + B\omega_r + J\frac{\mathrm{d}\omega_r}{\mathrm{d}t} \tag{17}$$

where T_m is the load torque; B is the friction coefficient; ω_r is the mechanical angular velocity; J is the total moment of inertia of the rotor and the external load.

5.1.2. Control model of PMSM

The PMSM entity used in this paper is controlled by the dual closed-loop Field-Oriented Control (FOC) method with $i_d = 0$ A. The external rotation speed and torque measured from actual PMSM are used as the input to the control system to drive the PMSM DT. The PMSM DT electrical status can be controlled by means of a physical rotation speed signal and torque condition (see Fig. 5).

Now there are a variety of control methods for PMSM, such as Model Predictive Control (MPC), ML-assisted methods, etc. In this paper, only PI control in the actual PMSM object is used as a part in the DT. The study of PMSM control methods is not included in this paper.

5.1.3. Power loss model of PMSM

Copper, iron and magnetic losses are the main causes of PMSM heating. The calculation model of copper loss is

$$P_{\mathrm{Cu}} = \frac{3}{2} i_q^2 R \tag{18}$$

where i_q is the result of the constant amplitude transformation, so its RMS value needs to be divided by $\sqrt{2}$.

Commonly used the calculation methods for analyzing iron and magnetic losses in PMSM include empirical formulas and Finite Element Method (FEM). However, empirical formulas often involve complex non-linear links and numerous parameters that are inconvenient to measure directly, such as eddy current density and conductivity.[31] Moreover, discrepancies in parameter values can lead to deviations between calculated and actual results. To overcome these challenges and achieve higher accuracy, the model-driven method is selected for analyzing the loss in PMSM.

This paper uses the experiment and FEM analysis tool Maxwell to conduct 121 sets (5–15 N·m; 1000–2800 r/min) simulation near the rated working conditions (10 N·m, 2500 r/min) of the PMSM (see Fig. 6).

The three graphs presented above depict the iron loss, magnetic loss, and copper loss of the PMSM with various rotation speeds and torque conditions. Observing the graphs, it is evident that the iron and magnetic losses of the PMSM demonstrate a robust correlation with the rotation speed, while the copper loss exhibits a strong correlation with the torque applied. Moving on to the three graphs below, they showcase the input power, output power, and the error between them (input power - output power).

Based on the relationship observed between iron and magnetic losses, which is related to the rotation speed and torque, a quadratic linear formula is fitted to establish a data-driven model for the iron and magnetic losses of the PMSM. The resulting data-driven model can be represented as follows:

$$\begin{cases} P_{\mathrm{Iro}} = L_1(i_q, \omega_r) \\ P_{\mathrm{Mag}} = L_2(i_q, \omega_r) \end{cases} \tag{19}$$

where P_{Iro} and P_{Mag} represent the iron loss and magnetic loss, respectively; ω_r represents the rotation speed; L_1 and L_2 represent the function of iron loss and magnetic loss.

Additionally, the normal distribution of the power error is verified using a Q-Q plot. The analysis reveals that the error between the input and output power follows a normal distribution with a mean of 0. This confirms the acceptability of the power loss model derived from the FEM calculations of iron, magnetic and copper losses (see Fig. 7).

5.1.4. Thermal model of PMSM

Similar to electrical resistance, heat transfer in PMSM is impeded by various structures, which can be referred to as thermal resistance. The value of thermal resistance is typically determined by the material and dimensions of the corresponding structure. To accurately model the thermal behavior of the PMSM, an online thermal model has been developed based on the Mellor thermal network, considering the radial and axial

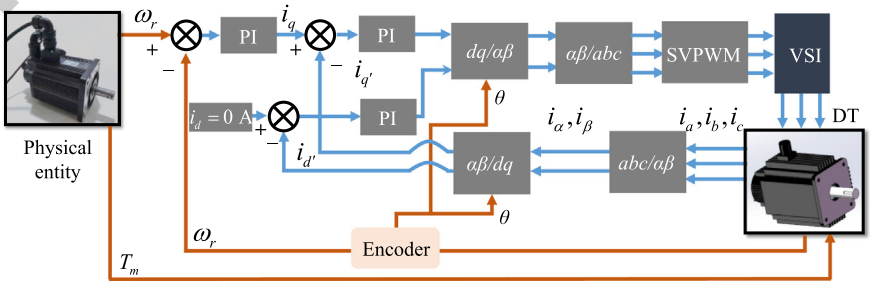

Electrical, control and dynamics model of PMSM

Fig. 5 Control method of DT interaction with entity PMSM.

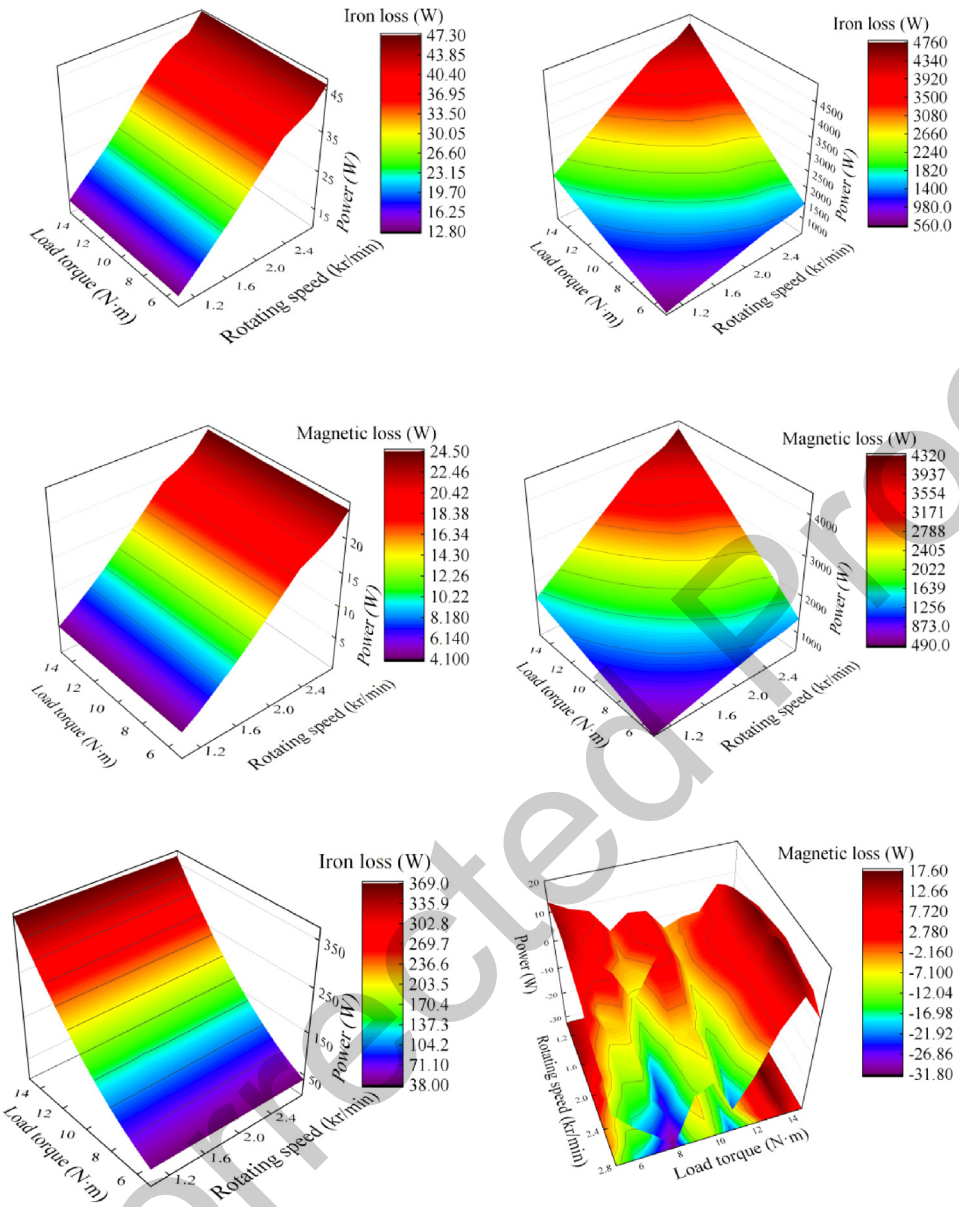

Fig. 6 Loss and power of PMSM.

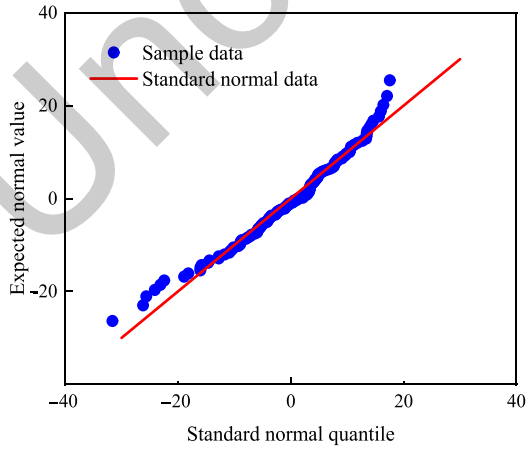

Fig. 7 Verification of normal distribution of power error.

directions. This model incorporates the actual material properties and dimensions of the PMSM components, including thermal resistance, nodes, heat sources, and air ends (see Fig. 8).

The nodes in the thermal network are assigned numbers based on the location of the different thermal resistances, facilitating the analysis and calculation process. Each node represents a specific point in the PMSM where heat can flow. Between every two nodes, there exists a distinct thermal resistance (designated as Y_{**}). The point at the end of the thermal network that contacts the air is labeled as node 0, representing the actual air temperature. While every structure in the thermal network possesses a heat capacity, it only has impacts on the rate of temperature change, but not on the calculation and analysis itself. Hence, for ease of calculation and analysis, the links representing the heat capacity in the thermal network are omitted.

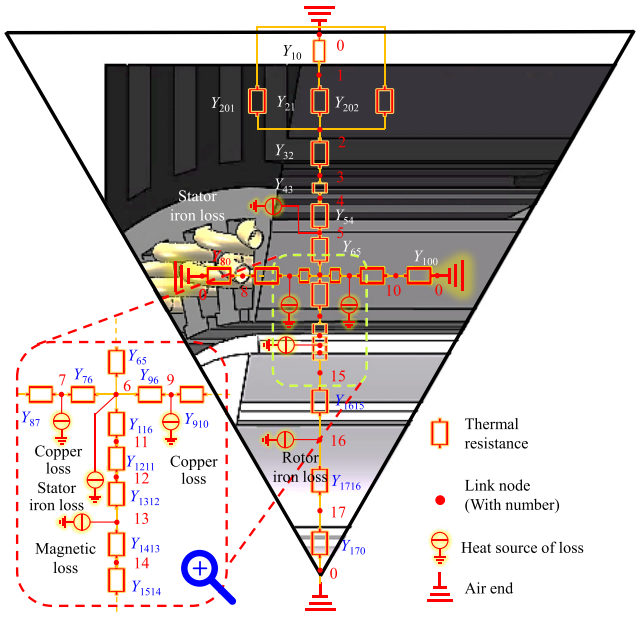

Fig. 8 Schematic diagram of PMSM thermal network structure.

The primary sources of heat within the PMSM are the iron, copper, and magnetic losses. When considering steady heat generation, these losses can be likened to current sources in an electrical circuit. Based on the specific locations of these heat sources, we assign nodes 5, 6, 7, 9, 13, and 16 to represent their respective heat source locations within the thermal network.

To enable real-time temperature calculations for each node in the PMSM, we draw a comparison between the PMSM's thermal network and a power grid, and employ the admittance matrix algorithm, commonly used in power system analysis, to achieve real-time monitoring of the temperature for each node within the thermal network. This approach allows for accurate and timely temperature estimation in the PMSM during operation (see Fig. 9).

According to the PMSM structure, we establish a framework consisting of 17 nodes to represent the temperature at various locations within the PMSM. In Fig. 9, nodes 5, 6, 7, 9, 13, and 16 within the heat source vector on the left side denote the input points for heating power related to iron, magnetic, and copper losses. The remaining nodes are set to zero, indicating no heat source at those locations. The unit of the heat source vector is measured in Watts.

The matrix shown in the middle of Fig. 9 represents the admittance matrix associated with the PMSM. Each element in the matrix corresponds to the admittance of the respective thermal resistance in the thermal network, which is essentially the reciprocal of the thermal resistance. This matrix is a large 17×17 sparse diagonal matrix, where all elements except for the identified ones are set to 0. The element highlighted in yellow within the matrix represents the admittance at the corresponding heat source. On the right side, the node temperature vector represents the temperatures of the 17 nodes relative to the air end point, which is designated as 0. The unit of temperature for all nodes is Kelvin. The unit of the elements in the admittance matrix is Watts per Kelvin.

Additionally, the Temperature Coefficient of Resistance (TCR) is defined as

$$\mathrm{TCR} = \frac{R_2 - R_1}{R_1(T_2 - T_1)} \tag{20}$$

where R_1 and R_2 is the thermal resistance at T_1 and T_2, respectively; TCR is around 0.004 at 25 °C (common metal). The material and size inside the PMSM will not change. When the PMSM works stably, there will not be such a large temperature change during stable operation. In other words, the influence of thermal resistance on Y_{**} can be ignored.

According to the first-principle structure of dynamic DT, the input is $\boldsymbol{U} = [\omega_r, T_m]$; $\boldsymbol{D}$ is disturbance $[\delta_d, \delta_q]$; $c_j(t)$ is the working condition (temperature, etc.); internal time-varying parameters of the model are $x_m = \{\psi_f, R, L_d, L_q\}$; the static parameters are $x_n = \{P_n, B, J, Y_{**}\}$ and the inner parameters in Eq. (19); DT output are $\hat{\boldsymbol{O}} = [i_d, i_q, u_d, u_q]$. Therefore, the multi-field coupling model of PMSM DT can be described as

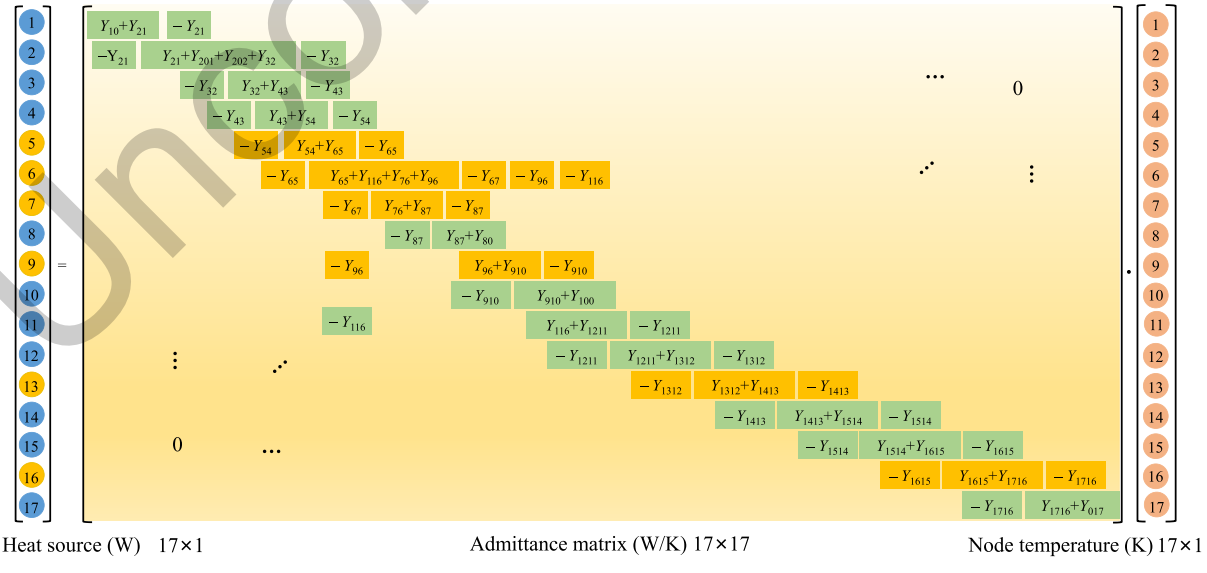

Fig. 9 Admittance matrix of entire thermal network of PMSM.

$$\boldsymbol{T} = [Y_{**}] \cdot \begin{bmatrix} P_{\mathrm{Cu}}([\tau(\psi_f, R, L_d, L_q, P_n, B, J, \omega_r, T_m)] + (\delta_d, \delta_q)) \\ P_{\mathrm{Iro}}([\tau(\psi_f, R, L_d, L_q, P_n, B, J, \omega_r, T_m)] + (\delta_d, \delta_q)) \\ P_{\mathrm{Mag}}([\tau(\psi_f, R, L_d, L_q, P_n, B, J, \omega_r, T_m)] + (\delta_d, \delta_q)) \end{bmatrix} \tag{21}$$

where $\tau(\cdot)$ represents the model of the PMSM, which includes electrical, control, and dynamic aspects (see Eq. (15)); P_{Cu}, P_{Iro} and P_{Mag} represent the power loss at the given input and corresponding operating conditions; $[Y_{**}]$ represents the admittance inverse matrix of the PMSM, which is then used to determine the temperature $\boldsymbol{T}$ of each node in the PMSM. In Eq. (21), the dimensions of the matrices on the right side of the equation need to be adjusted according to the actual structure and specific conditions of the system. The heat source vectors provided are intended for illustrative purposes only. They serve as examples to demonstrate the concept of heat sources in the system. In practice, the actual heat source vectors would be specific to the particular system be analyzed or implemented.

In this paper, we establish a PMSM DT based on a combination of model-driven and data-driven methods. In terms of the electrical, control, power and temperature of the PMSM, we use the model-driven way; as the power loss of the PMSM's mathematical model is nonlinear and complex, the results under multiple working conditions are used to build data-driven power loss model. Through the combination of the models of the two forms, DT can be further enriched to more comprehensively reflect the multidisciplinary coupling operation status of PMSM under different working conditions, and provide a more reliable basis for subsequent analysis and decision making.

5.2. Dynamic update mechanism of PMSM DT

5.2.1. Abnormal detection

The electronic components within actual equipment deteriorate or eventually fail as the operating time increases. To determine potential abnormalities, this paper select the input power as a trigger index according to the Independence Principle. Because the input power is neither the model's output nor an internal critical parameter in the PMSM system, the trigger is defined as the ratio of the power error between the initial moment and the present moment, as shown in Eq. (22).

$$\mathrm{trig} = \frac{P^0_{\mathrm{entity}} - P_{\mathrm{DT}}}{P^t_{\mathrm{entity}} - P_{\mathrm{DT}}} \tag{22}$$

where P^0_{entity}, P^0_{entity} and P_{DT} are the input power of the entity at the initial time, time t and DT, separately; trig is abnormal trigger. The input power of an entity PMSM is usually large than the input power calculated by DT due to additional power losses (e.g., air friction loss).

The increase in power resulting from demagnetization is significantly higher compared to that caused by resistance changes. When the set threshold is not met, the abnormal trigger will be initiated, indicating the need to update the DT.

5.2.2. Dynamic update of DT

Online measurement is hard when used to update the flux linkage value, and the magnetic field sensor is expensive. Moreover, the compact structure of PMSM is not convenient to measurement.

Therefore, we perform online parameter estimation for the d-q voltage model of PMSM by the RLS algorithm with forgetting factor. This paper adopts the RLS, and realizes the function of online dynamic integration update parameters. In surface-mount PMSM, $L_d = L_q = L$. When the PMSM works stably, the d-q voltage models of the PMSM are be written as

$$\begin{cases} u_d = -\omega_e i_q L + \delta_d \\ u_q = [\, i_q \quad -\omega_e \,] \begin{bmatrix} R \\ \psi_f \end{bmatrix} + \delta_q \end{cases} \tag{23}$$

According to the updated RLS Eq. (8), in the d-axis formula, $-\omega_e i_q$ corresponds to the $\boldsymbol{Q}_t$ term, u_d corresponds to the $\boldsymbol{Z}_t$, term, and L is the $\boldsymbol{\theta}$ to be identified; in the q-axis formula, i_q and ω_e correspond to the $\boldsymbol{Q}_t$ term, u_q corresponds to the $\boldsymbol{Z}_t$ term, and R, ψ_f are the $\boldsymbol{\theta}$ to be identified. $\boldsymbol{V}_t$ is the random indeterminate item (δ_d, δ_q).

Taking u_d (in Eq. (23)) as an example, the estimation algorithm of RLS parameters is

$$\begin{cases} \boldsymbol{K}_{t+1} = \boldsymbol{P}_{t+1}\left(-\omega_e i_q\right)^{\mathrm{T}}(t+1) \times \left[\lambda + \left(-\omega_e i_q\right)\boldsymbol{P}_i\left(-\omega_e i_q\right)^{\mathrm{T}}\right]^{-1} \\ \boldsymbol{P}_{t+1} = \frac{1}{\lambda}\left[\boldsymbol{P}_t - \boldsymbol{K}_{t+1}\left(-\omega_e i_q\right)\boldsymbol{P}_t\right] \\ \hat{L}_{t+1} = \hat{L}_t + \boldsymbol{K}_{t+1}\left[U_d(t+1) - \left(-\omega_e i_q\right)\hat{L}_t - \delta_q\right] \end{cases} \tag{24}$$

By setting the corresponding initial value of $\boldsymbol{K}$,$\boldsymbol{P}$ and λ, an estimate of L in the current state can be obtained after iteration.

5.2.3. Consistent measurement

We define PMSM state vectors and a set of vectors as follows:

$$\begin{cases} \boldsymbol{s}_w = \left[u_{qw}, u_{dw}, i_{qw}\right]^{\mathrm{T}} \\ \boldsymbol{X} = [\boldsymbol{s}_1, \boldsymbol{s}_2, \boldsymbol{s}_3, \boldsymbol{s}_{\mathrm{DT}}] \end{cases} \tag{25}$$

where $\boldsymbol{s}_w$ represents the measured state matrix of w measurements of u_q, u_d and i_q of the PMSM entity; $\boldsymbol{s}_{\mathrm{DT}}$ is the running state vector value of DT; $\boldsymbol{X}$ consists of DT and three entity state vectors under the same working condition. The mean of these three entity state vectors is defined as

$$\boldsymbol{\mu}_\alpha = \frac{1}{3}(\boldsymbol{s}_1 + \boldsymbol{s}_2 + \boldsymbol{s}_3) \tag{26}$$

Therefore, the MD between PMSM and DT is

$$\mathrm{MD} = \sqrt{(\boldsymbol{\mu}_\alpha - \boldsymbol{s}_{\mathrm{DT}})^{\mathrm{T}}\boldsymbol{D}(\boldsymbol{\mu}_\alpha - \boldsymbol{s}_{\mathrm{DT}})} \tag{27}$$

5.2.4. Overall algorithm for PMSM DT dynamic update

There is not a standard for the selection of MD and trig values, which need to be determined according to the specific object and the different tolerance for DT deviation. In this paper, the upper limit value of MD is set to 2.5, and the lower limit value of trig is set to 0.97. The whole DT update algorithm is as shown as Algorithm 1.

Please cite this article in press as: GUO H et al. Dynamically updated digital twin for prognostics and health management: Application in permanent magnet synchronous motor, *Chin J Aeronaut* (2024), https://doi.org/10.1016/j.cja.2023.12.031

Algorithm 1. Online dynamic DT update algorithm of PMSM

Input $U_{\text{phase}}, I_{\text{phase}}$, Output ψ_f, R, L, Initialization of $P_{\text{DT}}, P^0_{\text{entity}}$ and trig $= P^0_{\text{entity}} - \frac{P_{\text{DT}}}{P^t_{\text{entity}} - P_{\text{DT}}}$

1. Abnormal detection

while trig < 0.97 **do** calculate power factor

$V \overset{\text{add}}{\leftarrow} \text{voltage}^2[i], C \overset{\text{add}}{\leftarrow} \text{current}^2[i], P \overset{\text{add}}{\leftarrow} \text{voltage}[i] \times \text{current}[i], \omega_e = P_n \omega_r$

Calculate power factor using root mean square method

$V_{\text{rms}} = \sqrt{V/N}, C_{\text{rms}} = \sqrt{C/N}, P = P/N,$

$i_q = \sqrt{2} I_{\text{phase}}, \text{fact} = P/V_{\text{rms}}/C_{\text{rms}}$

$u_q = U_{\text{phase}} \cos(\text{fact}), u_d = U_{\text{phase}} \sqrt{1 - \cos^2(\text{fact})}$

2. Parameter estimation

for each u_q, u_d, i_q, ω_e

$u_d = -\omega_e i_q L$

$u_q = R i_q + \omega_e \psi_f$

return ψ_f, R, L

3. Consistent Measurement

$\boldsymbol{s}_1 = [u_{q1}, u_{d1}, i_{q1}]^{\text{T}}, \boldsymbol{s}_2 = [u_{q2}, u_{d2}, i_{q2}]^{\text{T}}$

$\boldsymbol{s}_3 = [u_{q3}, u_{d3}, i_{q3}]^{\text{T}}, \boldsymbol{s}_{\text{DT}} = [u_{q\text{DT}}, u_{d\text{DT}}, i_{q\text{DT}}]^{\text{T}}$

$\boldsymbol{X} = [\boldsymbol{s}_1, \boldsymbol{s}_2, \boldsymbol{s}_3, \boldsymbol{s}_{\text{DT}}]$

$\boldsymbol{D} = \text{Cov}(\boldsymbol{X}^{\text{T}})^{-1}, \boldsymbol{\mu}_\alpha = (\boldsymbol{s}_1 + \boldsymbol{s}_2 + \boldsymbol{s}_3)/3$

$\text{MD} = \sqrt{(\boldsymbol{\mu}_\alpha - \boldsymbol{s}_{\text{DT}})^{\text{T}} \boldsymbol{D} (\boldsymbol{\mu}_\alpha - \boldsymbol{s}_{\text{DT}})}$

if MD < 2.5 **then**

$P^0_{\text{Real}} = P^t_{\text{Real}}$

break

The working mechanism of multi-field coupling PMSM DT with dynamic update capability is shown in Fig. 10.

5.3. Verification of PMSM DT and its demagnetization trend prediction experiment

5.3.1. Establishment of a system of PMSM DT

In this paper, the DT system of PMSM is established and validation through the workflow of the Model in the Loop (MIL), Software in the Loop (SIL), and Hardware in the Loop (HIL). DT is encapsulated as a dynamic-link library (DLL) that can be run online. The main parameters of the PMSM this paper used are shown in Tables 1, 2, and 3.

The main equipment of the experiment bench is PMSM, torque sensor, rotation load, speed sensor and the PMSM DT PHM system (see Fig. 11, from left to right). The other devices are the rotation load controller, PMSM controller, current sensor, voltage sensor, capture card, and temperature sensors located at the PMSM shell.

5.3.2. Comparison of the electrical state of PMSM entity and DT

The voltage and current characteristics are important criteria to measure the similarity between the PMSM entity and its DT. In this paper, the electrical parameters of the PMSM with a torque of 4 N · m, 6 N · m and 8 N · m and a speed in the range from 1000 r/min to 1600 r/min are compared with its DT electrical parameters (see Fig. 12).

It can be seen from Fig. 12 that under the three torque conditions, the results of the input line voltage of the PMSM entity and the DT are very close, and the line current of the PMSM entity and the DT have the almost the same error under the same working conditions. Although there is a certain error, we can still consider the DT to be reliable.

5.3.3. Comparison of the thermal state of PMSM entity and DT

In order to further verify the correctness of the thermal model, the same working conditions (air temperature 25 °C) was simulated by ANSYS Motor-CAD software (see Fig. 13). Finally, we compared the thermal model, the FEM simulation and the sensor measurement results (see Fig. 14).

Due to the limitation of the space structure of PMSM, the temperature sensor is arranged at the shaft and the shell. From Fig. 14, we noticed that the calculation results of the thermal model are generally consistent with the results of the FEM analysis, which shows the accuracy of the thermal model. By comparing the electrical and temperature parameters of the entity and its DT, the correctness of the multi-field coupling DT of PMSM is proved.

5.3.4. Comparison of PMSM DT update algorithm accuracy

Parameter estimation is an important part of DT update. The lack of model uncertainty (δ_d, δ_q) will introduce large errors

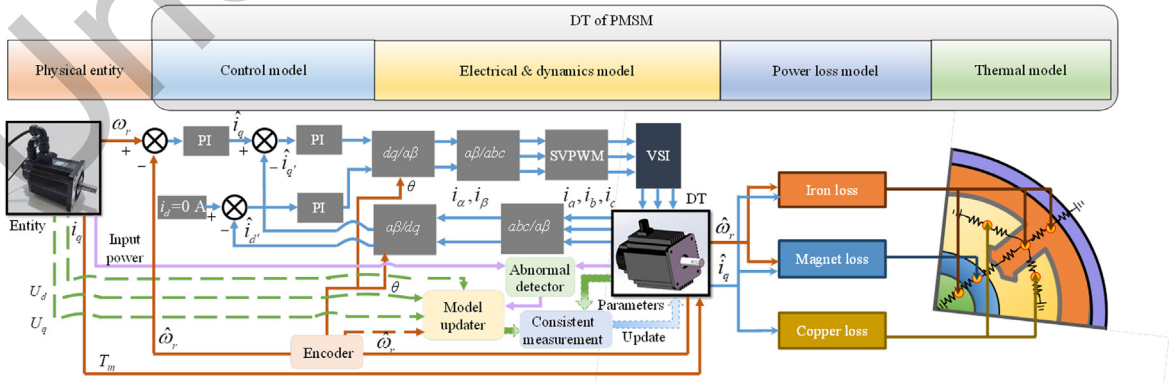

Fig. 10 Dynamically updated multi-field coupling DT of PMSM.

Table 1 Size parameters of PMSM.

Parameter	Value
Number of pole pairs	4
Number of stator slots	36
Polar arc coefficient	0.85
Moment of inertia (kg·m^2)	1.94×10^{-3}
Stator outer diameter (m)	1.22×10^{-1}
Stator inner diameter (m)	7.8×10^{-2}
Rotor outer diameter (m)	7×10^{-2}
Shaft diameter (m)	2.2×10^{-2}
Magnet thickness (m)	3×10^{-3}

Table 2 Electrical parameters of PMSM.

Parameter	Value
Stator resistance (Ω)	3.65×10^{-1}
Inductance (H)	1.225×10^{-3}
Rotor flux (Wb)	1.53×10^{-1}
Rated power (W)	2.6×10^{3}
Rated current (A)	10
Rated rotational speed (r/min)	2500
Rated torque (N·m)	10

Table 3 Components & Material.

Component	Material
Stator and rotor	Silicon steel (DW315_50)
Permanent magnets	NdFeB_35
Wire winding	Copper
Shaft	Carbon steel

when using parameters identification method, which will affect the precision of DT. Therefore, the uncertainty of the model needs to be considered when identifying parameters.

By comparing the real value of ψ_f, R, L and the results obtained by using the RLS method that introduces model uncertainty, it is proved that this method can make high-precision estimation of entity (see Fig. 15).

5.3.5. Comparison of current change trend due to demagnetization

According to actual engineering experience, the long-term operating current of PMSM shall not exceed 1.1–1.5 times of its rated current value. Monitoring the trend of current changes due to demagnetization is necessary to analyze the RUL of PMSM. Based on the above criteria, this paper predicts the demagnetization trend of the entity without taking into account mechanical failures. We can monitor the rotor flux condition of the entity at all times using PMSM DT. Under the same working condition (1200 r/min, 6 N · m), we run the PMSM for a total of 800 h, and simultaneously record the line current of the PMSM (see Fig. 16).

Other recorded data from the experiment are presented in Table 4.

Since only the line voltage U_L and line current I_L can be measured from the actual PMSM, according to the constant amplitude relationship, here give the relationship between U_L, I_L and U_q,I_q as:

$$\begin{cases} U_L = \frac{\sqrt{6}}{2} U_q \\ I_L = \frac{\sqrt{2}}{2} I_q \end{cases}$$

It is evident that as the running time increases, the input current and power of both the entity and DT exhibit an increase. The voltage change in the entity does not show a distinct trend, whereas the voltage in the DT decreases. Due to the omission of various frictions present in the actual PMSM and the partial voltage of other components in the DT, there may be errors in the results for situations P_{entity} and P_{DT}. The parameters in Table 4 provide evidence that DT closely approximates the state of the entity.

By incorporating the abnormal factors observed in the experimental data, we can utilize Eq. (22) to analyze the demagnetization situation of the PMSM. Using the first correction as an example, the threshold calculated based on Eq. (28) using the abnormal indexes P_{entity} and P_{DT} is

$$\frac{P_{\text{entity}}^{i_1} - P_{\text{DT}}}{P_{\text{entity}}^{i_0} - P_{\text{DT}}} = \frac{790.014 - 855.790}{787.979 - 855.790} = 0.9699 < 0.97 \tag{28}$$

At this juncture, Eq. (28) signifies that the DT has surpassed the allowable deviation from the entity, necessitating an update of the DT. The all three correction values and time of PMSM DT flux are recorded, as shown in Table 5.

Autoregressive Integrated Moving Average (ARIMA) is a popular method used for time series forecasting. Its underlying

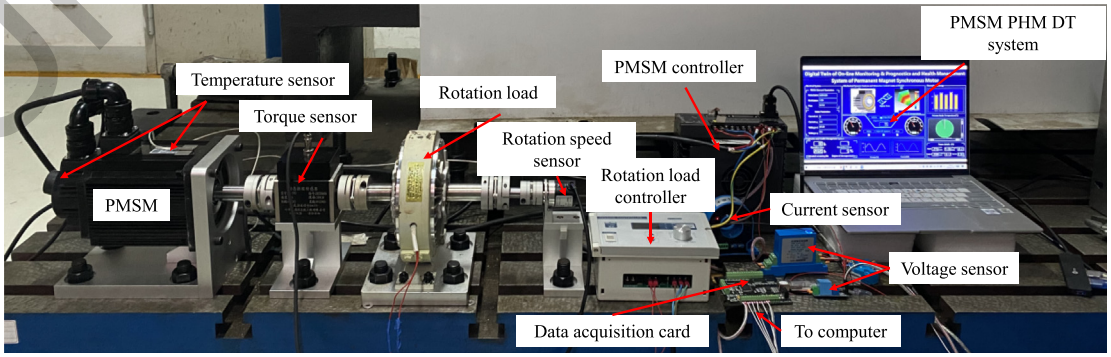

Fig. 11 Experiment bench of PMSM DT system.

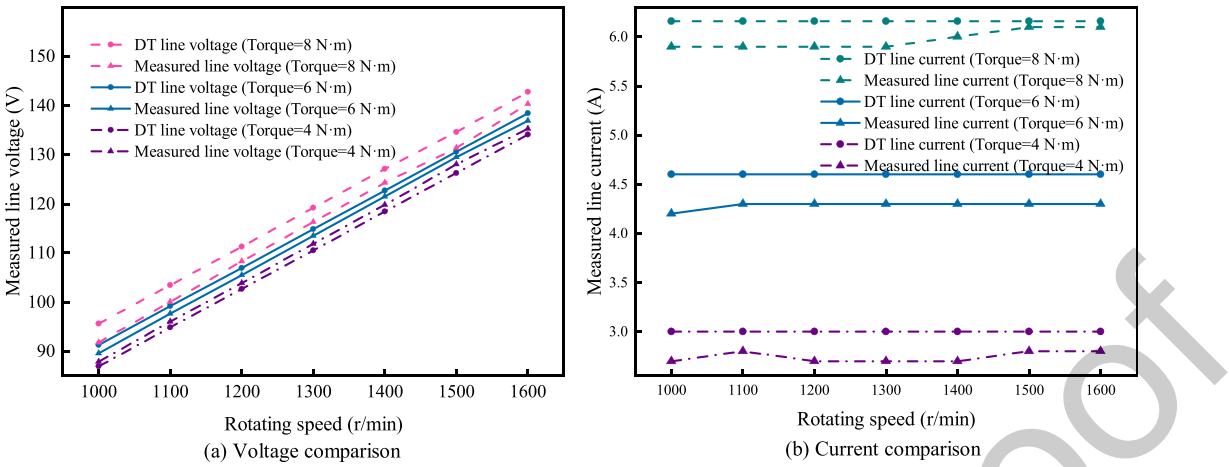

Fig. 12 Comparison of electrical parameters of PMSM entity and DT.

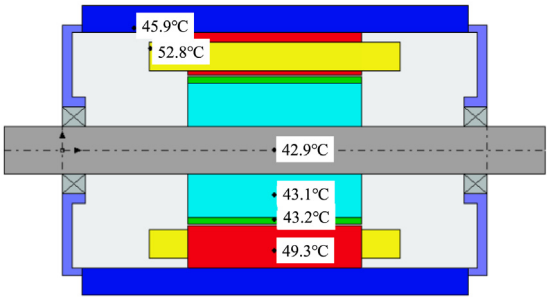

Fig. 13 Thermal simulation results of PMSM.

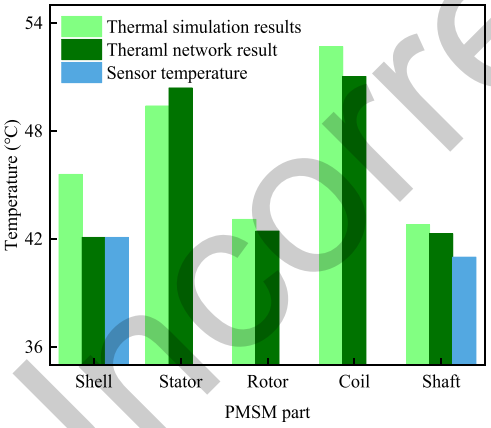

Fig. 14 Comparison of temperature results of simulation, DT thermal model and sensors (1200 r/min, 6 N·m).

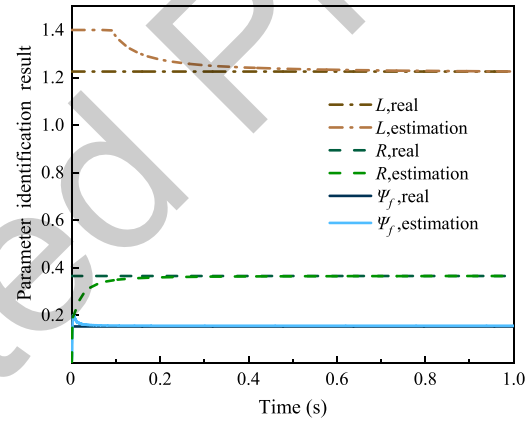

Fig. 15 Results of PMSM parameters identification.

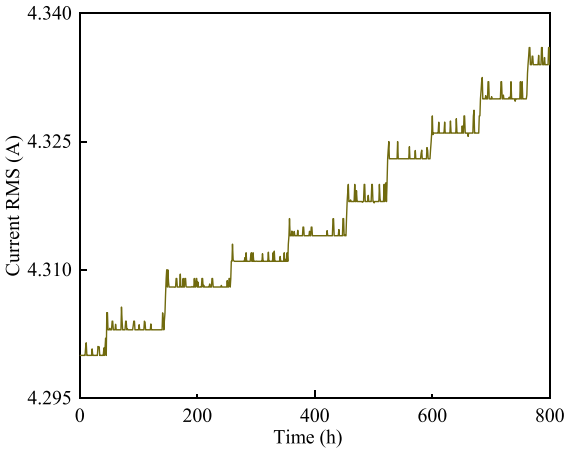

Fig. 16 RMS data of original current.

principle involves regression analysis using historical data and error data. The ARIMA requires the data to be stationary, thus necessitating the application of differencing techniques to the original current data. As the working time progresses and vibration damage accumulates, the magnetism of the rotor will undergo irreversible changes. The prediction result of the ARIMA model based on the current signal is shown in Fig. 17.

This model predicts the current from 690 to 810 h according to the ARIMA model. The predicted data are fitted in the form of a quadratic function as follows:

$$i_{\text{pred}}(t) = 6.215 \times 10^{-7} t^2 - 8.5 \times 10^{-4} t + 4.6177 \quad (29)$$

Table 4 Correction parameters and time of PMSM entity and DT.

Item	Runtime (h)	U_L(V)	I_L(A)	P_{entity}(W)	$\hat{U}_q$(V)	$\hat{I}_q$(A)	P_{DT}(W)
t_0	0	105.800	4.300	787.979	87.290	6.536	855.790
t_1	259	105.803	4.311	790.014	87.120	6.550	855.954
t_2	524	105.800	4.323	792.194	86.940	6.570	856.794
t_3	764	105.873	4.335	794.943	86.770	6.588	857.460

Table 5 Correction value and time of PMSM DT flux.

Item	Value (Wb)	Runtime (h)
Initial value	0.153	0
First correction	0.1526	259
Second correction	0.1522	524
Third correction	0.1518	764

Curve fitting is also a method for approximating discrete data with analytical expressions. However, when fitting the original data, there may be several difficulties. For example, the signal collected by the sensor will be polluted by noise, and curve fitting is a challenge for data with complex changes. But the data obtained from the DT model is more accurate. According to the data of PMSM DT in Table 5, the demagnetization fitting curve of the PMSM DT is obtained as seen in Fig. 18.

In the experiments, due to the stability and reliability of PMSM, the consistency of DT and entity characteristics can be ensured only through parameter updates. Here, we represent the health state by using flux values as

$$H = 1 - \frac{\Delta\psi_f^t}{\psi_f^{\text{threshold}}} = 1 - \frac{\psi_f^0 - \psi_f^t}{\psi_f^{\text{threshold}}} \tag{30}$$

where $\Delta\psi_f^t$ is the flux variation value at time t, $\psi_f^{\text{threshold}}$ is the threshold value of the flux, ψ_f^0 is the initial flux value, and ψ_f^t is the flux value at time t.

According to the design requirement, PMSM will malfunction if the demagnetization value exceeds 5%. In the case study, the initial flux value is $\psi_f^0 = 0.153$ Wb, so the threshold value of the flux is $\psi_f^{\text{threshold}} = 0.153 \times 0.05$ Wb. The flux value at current time is 0.1518 Wb. Therefore, the health status indicator can be obtained as follows:

$$H = 1 - \frac{0.153 - 0.1518}{0.153 \times 0.05} \approx 0.843 \tag{31}$$

At this point, through the update algorithm, the magnetic flux value in DT has been updated from the original 0.153 to 0.1518 Wb according to the PMSM current health state by using the RLS method. Therefore, based on assessment of the health factors, we consider the PMSM to be in a minor fault state. If the PMSM continues to operate, the flux will further degrade, and we can define it as in moderate fault or even more severe fault state based on the actual condition of the PMSM.

Here, we focus on the updating of demagnetization $\psi_{\text{DT}}(t)$ from the normal state ($H = 1$) to the minor fault state ($H = 0.843$). If PMSM continues to operate, the corresponding DT needs update from time to time according to the health factors from the minor fault to moderate fault states ($H < H_1$). Fig. 18 shows the updated DT form the normal to minor fault states.

After curve fitting, the demagnetization function of PMSM DT is shown as follows:

$$\psi_{\text{DT}}(t) = -5.716 \times 10^{-10} t^2 - 1.3048 \times 10^{-6} t + 0.153 \tag{32}$$

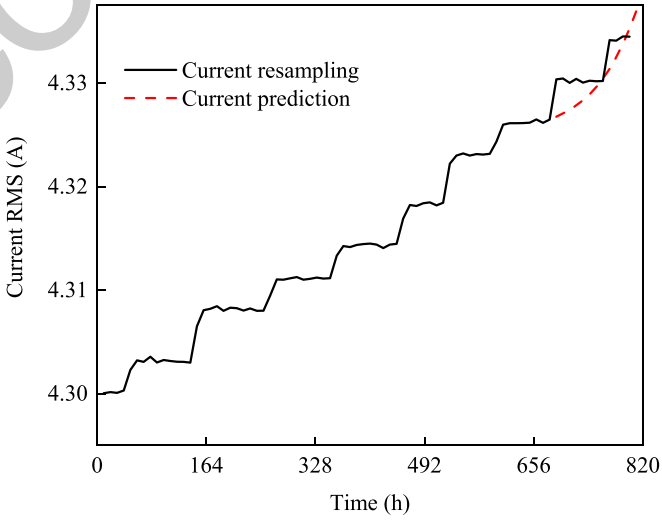

Fig. 17 Prediction result with ARIMA model.

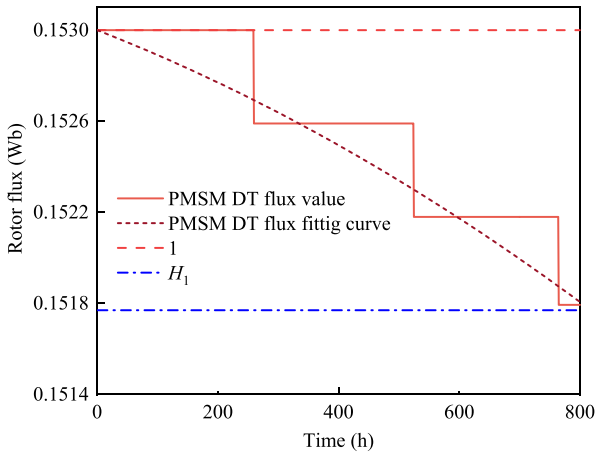

Fig. 18 PMSM DT demagnetization and its fitting curve.

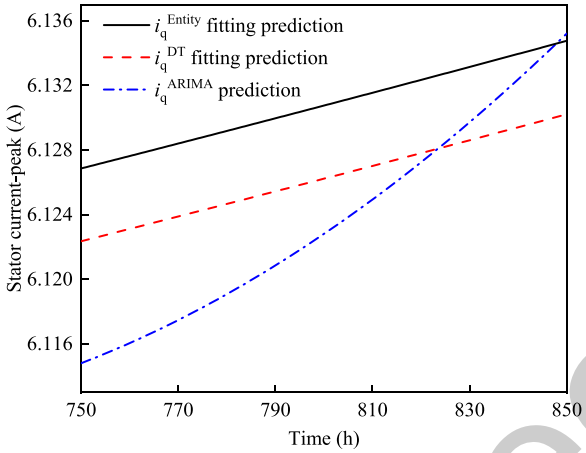

Fig. 19 Comparison of predicted results of current with three methods.

We also fit the current original data. The fitting curve of the data collected from the entity is

$$i_{\text{Entity}}(t) = 1.659 \times 10^{-8} t^2 + 2.935 \times 10^{-5} t + 4.301 \tag{33}$$

The control model in PMSM uses a constant amplitude transformation for three-phase alternating current. The entity acquisition data and the data used for ARIMA prediction are the RMS values of the current signal. Therefore, the i_q in DT is $\sqrt{2}$ times that of the RMS value of the current acquired by the sensor. According to the relationship between the current and the rotor flux in Eq. (16), the trend curve of i_q can be obtained in the three different methods shown as follows:

$$\begin{cases} i_q^{\text{ARIMA}}(t) = \sqrt{2} i_{\text{pred}}(t) \\ i_q^{\text{DT}}(t) = \frac{T_e}{1.5 P_n \psi_{\text{DT}}(t)} \\ i_q^{\text{Entity}}(t) = \sqrt{2} i_{\text{Entity}}(t) \end{cases} \tag{34}$$

Finally, comparison of the prediction results of i_q with the three different methods in the interval of 750–850 h is performed (see Fig. 19).

As shown in Fig. 19, i_q^{DT} is closer to the actual curve. More importantly, the high-precision prediction curve obtained by DT is obtained from only 4 sets of data. The data resource consumption is reduced by 200 times. More importantly, according to the error area calculation in Fig. 19, the error of DT-based demagnetization trend prediction during this time period is reduced by about 37% compared with the traditional time series prediction error.

To sum up, the PHM based on DT is superior to traditional fitting forecasting and time series forecasting in both accuracy and efficiency. Compared with the traditional maintenance method, consumption of computing resources is reduced.

6. Conclusions

(1) This paper proposes a dual loop DT based PHM framework to account for the differences between the normal state DT and degradation DT of the product.
(2) A structure of first-principle dynamic DT is proposed under the normal condition.
(3) The "Independence Principle" is proposed to select appropriate trigger between DT and physical entity during lifecycle degradation.
(4) The dynamic multi-field coupling DT of PMSM is established. Experimental results show that the DT-based PHM approach reduces the error in degradation prediction results by approximately 37% compared to traditional time series-based forecasting methods.

Declaration of competing interest

The authors declare that they have no known competing financial interests or personal relationships that could have appeared to influence the work reported in this paper.

Acknowledgements

This study was co-supported by the National Natural Science Foundation of China (Nos. U2233212; 51875014), Beijing Natural Science Foundation, China (No. L221008), and the China Scholarship Council (No. 202106020001).

References

1. Cheng JF, Zhang H, Tao F, et al. DT-II: Digital twin enhanced industrial internet reference framework towards smart manufacturing. *Robot Comput Integr Manuf* 2020;**62**:101881.
2. Grieves M. Digital twin: Manufacturing excellence through virtual factory replication [Internet]. 2015. Available from: http://www.apriso.com/library/Whitepaper_Dr_Grieves_DigitalTwin_ManufacturingExcellence.php.
3. Qi QL, Zhang H, Tao F, et al. Theory and key technologies of digital twin interaction. *Computer Integrated Manufacturing System* 2023.01.001 [Chinese].
4. Li LN, Aslam S, Wileman A, et al. Digital twin in aerospace industry: a gentle introduction. *IEEE Access* 2021;**10**:9543–62.
5. Tao F, Sun XM, Cheng JF, et al. MakeTwin: a reference architecture for digital twin software platform. *Chin J Aeronaut* 2023.
6. Bernard M. The best examples of digital twins everyone should know about [Internet]. 2022. Available from: https://www.forbes.com/sites/bernardmarr/2022/06/20/the-best-examples-of-digital-twins-everyone-should-know-about/?sh=70dc6f1e225f/.

7. Siemens. For a digital twin of the grid siemens solution enables a single digital grid model of the finnish power system [Internet]. 2017. Available from: https://www.siemens.com/press/pool/de/events/2017/corporate/2017-12innovation/inno2017-digitaltwin-e.pdf.
8. Martin L. Autonomic logistics information system (ALIS): Maintaining sustaining critical F-35 lightning ii systems [Internet]. 2016. Available from: https://www.lockheedmartin.com/content/dam/lockheed-martin/rms/documents/alis/CS00086-55%20(ALIS%20Product%20Card).pdf.
9. Tao F, Qi QL. Make more digital twins. *Nature* 2019;**573**(7775):490–1.
10. Tao F, Zhang H, Liu A, et al. Digital twin in industry: State-of-the-art. *IEEE Trans Ind Inf* 2019;**15**(4):2405–15.
11. Fan YP, Yang JZ, Chen JH, et al. A digital-twin visualized architecture for Flexible Manufacturing System. *J Manuf Syst* 2021;**60**:176–201.
12. Dang HV, Tatipamula M, Nguyen HX. Cloud-based digital twinning for structural health monitoring using deep learning. *IEEE Trans Ind Inform* 2022;**18**(6):3820–30.
13. Castellani A, Schmitt S, Squartini S. Real-world anomaly detection by using digital twin systems and weakly supervised learning. *IEEE Trans Ind Inform* 2020;**17**(7):4733–42.
14. Wang QY, Jiao WH, Zhang YM. Deep learning-empowered digital twin for visualized weld joint growth monitoring and penetration control. *J Manuf Syst* 2020;**57**:429–39.
15. Venkatesan S, Manickavasagam K, Tengenkai N, et al. Health monitoring and prognosis of electric vehicle motor using intelligent-digital twin. *IET Electr Power Appl* 2019;**13**(9):1328–35.
16. Moghadam FK, Nejad AR. Online condition monitoring of floating wind turbines drivetrain by means of digital twin. *Mech Syst Signal Process* 2022;**162**:108087.
17. Li WH, Rentemeister M, Badeda J, et al. Digital twin for battery systems: cloud battery management system with online state-of-charge and state-of-health estimation. *J Energy Storage* 2020;**30**:101557.
18. Lei ZC, Zhou H, Hu WS, et al. Towards a web-based digital twin thermal power plant. *IEEE Trans Ind Inf* 2022;**18**(3):1716–25.
19. Hu MH, He Y, Lin XZ, et al. Digital twin model of gas turbine and its application in warning of performance fault. *Chin J Aeronaut* 2023;**36**(3):449–70.
20. Bai F, Quan HB, Yin RJ, et al. Three-dimensional multi-field digital twin technology for proton exchange membrane fuel cells. *Appl Energy* 2022;**324**:119763.
21. Ye YM, Yang QA, Zhang JG, et al. A reconfigurable dynamic Bayesian network for digital twin modeling of structures with multiple damage modes. *Theor Appl Mech Lett* 2023;**13**(4):100440.
22. Li QW, Jiang P, Li H. Prognostics and health management of FAST cable-net structure based on digital twin technology. *Res Astron Astrophys* 2020;**20**(5):67.
23. Angjeliu G, Coronelli D, Cardani G. Development of the simulation model for Digital Twin applications in historical masonry buildings: the integration between numerical and experimental reality. *Comput Struct* 2020;**238**:106282.
24. Liu L, Guo YG, Lei G, et al. Iron loss calculation for high-speed permanent magnet machines considering rotating magnetic field and thermal effects. *IEEE Trans Appl Supercond* 2021;**31**(8):1–5.
25. Aivaliotis P, Georgoulias K, Chryssolouris G. The use of digital twin for predictive maintenance in manufacturing. *Int J Comput Integr Manuf* 2019;**32**(11):1067–80.
26. Oluwasegun A, Jung JC. The application of machine learning for the prognostics and health management of control element drive system. *Nucl Eng Technol* 2020;**52**(10):2262–73.
27. Peng F, Zheng L, Peng YD, et al. Digital twin for rolling bearings: a review of current simulation and PHM techniques. *Measurement* 2022;**201**:111728.
28. Booyse W, Wilke DN, Heyns S. Deep digital twins for detection, diagnostics and prognostics. *Mech Syst Signal Process* 2020;**140**:106612.
29. Correa-Jullian C, Groth KM. Opportunities and data requirements for data-driven prognostics and health management in liquid hydrogen storage systems. *Int J Hydrog Energy* 2022;**47**(43):18748–62.
30. Candon M, Esposito M, Fayek H, et al. Advanced multi-input system identification for next generation aircraft loads monitoring using linear regression, neural networks and deep learning. *Mech Syst Signal Process* 2022;**171**:108809.
31. Liu L, Ba X, Guo YG, et al. Improved iron loss prediction models for interior PMSMs considering coupling effects of multiphysics factors. *IEEE Trans Transp Electrif* 2023;**9**(1):416–27.

Please cite this article in press as: GUO H et al. Dynamically updated digital twin for prognostics and health management: Application in permanent magnet synchronous motor, *Chin J Aeronaut* (2024), https://doi.org/10.1016/j.cja.2023.12.031